

Solid State Chemistry of Tungsten Oxide Supported on Alumina

S. SOLED, L. L. MURRELL, I. E. WACHS, G. B. McVICKER, L. G. SHERMAN, S. CHAN, N. C. DISPENZIERE, and R. T. K. BAKER

Exxon Research & Engineering Company, Annandale, NJ 08801

The strong interaction between WO_3 and a $\gamma-Al_2O_3$ support is monitored under high temperature reducing and oxidizing conditions by a combination of physical and spectroscopic techniques. Below monolayer coverage a difficult to reduce highly dispersed surface tungsten oxide complex exists, whereas at higher coverages a more easily reduced bulk like WO_3 species is also present. Dynamic structural changes of the supported phase occur during high temperature treatment.

Supports can no longer be considered inert carriers which act solely to disperse a metal or metal oxide and thereby increase effective surface area. In many cases the reactivity and the catalytic properties of supported and bulk phases differ dramatically. A plethora of work has appeared over the last few years describing the strong metal support interaction (SMSI) of Group VIII metals with a titania support (1). In the "SMSI" state, metals display a dramatically reduced H_2 and CO chemisorption ability. Controversy exists about the basis of SMSI and such diverse explanations as electron transfer and TiO_2 migration onto the metal are being argued (1,2).

Examples of supports modifying the properties of transition metal oxides have also appeared in the literature. Recent work points to iron oxide phases as important species in Fischer-Tropsch synthesis (3). Iron oxide supported on SiO_2 (4) and TiO_2 (5) resist reduction under conditions in which bulk iron oxide easily reduces. Thus supported iron oxide catalysts are potentially interesting Fischer-Tropsch catalysts. The extensive studies on ethylene polymerization catalysts suggests that chromium (VI) species exist on a SiO_2 surface at temperatures above which bulk chromic anhydride (CrO_3) decomposes (6).

Recent evidence points to a strong interaction between WO_3 and $\gamma-Al_2O_3$ (7-10). The interaction alters the physical and chemical properties of both WO_3 and $\gamma-Al_2O_3$. In this review, we

0097-6156/85/0279-0165\$06.00/0
© 1985 American Chemical Society

describe studies of WO_3 on $\gamma-Al_2O_3$ using such diverse techniques as controlled atmosphere electron microscopy (CAEM) (11), x-ray photoelectron spectroscopy (XPS or ESCA) (12), thermal gravimetry (TG) (13,14), and laser Raman spectroscopy (15) to examine the nature of the tungsten oxide-alumina interaction.

Experimental

In these studies, both powder samples and films were prepared. Powder samples of nominal 4, 6, 10, 25 and 60 wt.% tungsten oxides on $\gamma-Al_2O_3$ (Engelhard Inc., reforming grade, $180\text{ m}^2/\text{gm}$, 325 mesh) were prepared by the incipient wetness impregnation method by adding an aqueous solution of ammonium meta-tungstate to the alumina powder, drying at 100°C and calcining in air at 500°C for 16 hrs. For the Raman experiments, $\gamma-Al_2O_3$ obtained from Harshaw (Al-4104E, $220\text{ m}^2/\text{gm}$) or Engelhard, Inc., (reforming grade, $180\text{ m}^2/\text{g}$) were used as supports. The impact of calcination and steaming as a function of temperatures was systematically studied. Samples of pure WO_3 and $Al_2(WO_4)_3$ were obtained from Cerac. For the CAEM experiments, film specimens of alumina, approximately 50 nm in thickness, were prepared according to the method described previously (16). Electron diffraction examination of selected areas of the alumina film showed the predominant phase to be $\gamma-Al_2O_3$. Tungsten was introduced onto the alumina as an atomized spray of a 0.1% aqueous solution of ammonium meta-tungstate. The tungsten loadings ranged between 4-20 micromoles/ m^2 (which corresponds to 10 to 50 wt.% tungsten on a $\gamma-Al_2O_3$ of $100\text{ m}^2/\text{g}$).

TG measurements were conducted on a Mettler TA-2000C as described elsewhere (13). For TG reduction studies, samples of WO_3 on $\gamma-Al_2O_3$ were heated to 970°C (at $10^\circ/\text{min}$) in He and then held isothermally until constant weight was obtained. This pre-calcination step minimizes overlapping reduction and dehydroxylation weight losses. After cooling to room temperature, H_2 was introduced, and the samples were reheated to a temperature between 600° and 900°C (at $10^\circ/\text{min}$) and held isothermally for two hours. The sensitivity and stability of the thermobalance (0.05 mg) establishes a detection limit of 1 to 2% WO_3 reduction to W. Slight gray discolorations indicate small amounts of WO_3 reduction below the TG detection limit.

In situ x-ray photoelectron spectra (XPS or ESCA) were collected on a modified Leybold Heraeus LHS-10 electron spectrometer. A moveable stainless steel block allowed sample transfer in vacuum from a reactor chamber to the ESCA chamber. The intensities and binding energies of the $W\ 4f_{5/2,7/2}$ signals (Al $K\alpha$ radiation) were monitored and referenced to the Al 2p peak at 74.5 eV. The 10% WO_3 and 60% WO_3 on $\gamma-Al_2O_3$ powder samples were calcined in air at 500°C and at 950°C respectively for 16 hrs and then pressed (at 30 Mpa) onto a gold screen, which in turn was mounted on a moveable stainless steel block. These samples were calcined in situ at 500°C to clean the surfaces prior to analysis. For the reduction treatments, the samples were heated for five minutes at the desired temperature in flowing H_2 (25 cc/min.), cooled to 250°C in

H₂, evacuated and then transferred into the ESCA chamber. Three samples were investigated; a bulk WO₃ foil, 60 wt.% WO₃ on γ -Al₂O₃, and 10 wt.% WO₃ on γ -Al₂O₃.

The Raman spectrometer consisted of a triple monochromator (Instruments SA, Model DL203) equipped with holographic gratings and F4 optics. The spectrometer was coupled to an optical multichannel analyzer (Princeton Applied Research, Model OMA2) equipped with an intensified photodiode array detector cooled to 15°C. Each spectrum reported here was accumulated for about 100 sec or less. The digital display of the spectrum was calibrated to give 1.7 cm⁻¹/channel with the overall spectral resolution at about 6 cm⁻¹. An argon ion laser (Spectra Physics, Model 165) was tuned to the 514.5 nm line for excitation. A prism monochromator (Anaspec Model 300S) with a typical band width of 0.3 nm removed the laser plasma lines (16). A 0.2 gm sample was pelletized under 60 MPa pressure into a 13 mm diameter wafer for mounting on a spinning sample holder. The laser power at the sample location was set in the range of 1-40 mW. The scattered light was collected by a lens (F/1.2, f/55 mm) held at about 45° with respect to the excitation.

Results

CAEM. Controlled atmosphere electron microscopy (11) was used to observe the behavior of tungsten oxide particles supported on γ -Al₂O₃ films when heated at temperatures up to 1150°C in 0.7 kPa oxygen. The two specimens described in the Experimental section were heated at increasing temperatures and the specimen changes were recorded in real time on video tape (15). The detailed observations of the dynamic behavior of the different tungsten oxide phases on the γ -Al₂O₃ film as a function of temperature and tungsten oxide content will be described in the Discussion section.

Thermalgravimetry. γ -Al₂O₃ on programmed heating (10°/min) to 1100°C in the presence of oxygen, continuously lost weight as a result of dehydroxylation: the weight lost between 200 and 1100°C equaled about 3.5%. In addition, a weak exotherm with an onset near 1050°C occurred during the transition of γ -Al₂O₃ to α -Al₂O₃. A 10% WO₃ on γ -Al₂O₃ sample showed different behavior. When this sample was heated in an oxygen atmosphere, a larger exotherm occurred at 1050°C as a fraction of the Al₂O₃ support reacted with WO₃ to form Al₂(WO₄)₃. The formation of Al₂(WO₄)₃ was confirmed by X-ray diffraction measurements. Alumina not utilized in tungstate formation transformed predominantly to θ -Al₂O₃: only a trace of α -Al₂O₃ was produced. Thus, the presence of the tungsten oxide surface phase inhibits the transition of θ -Al₂O₃ to α -Al₂O₃.

TG experiments indicate that a surface tungsten oxide phase on alumina is difficult to reduce. Table I shows the degree of reduction (expressed as percent WO_3 reduced to W^0) as a function of WO_3 loading after two hour reductions at 600 or 900°C. A 10% WO_3 on alumina sample was reduced at several intermediate temperatures as well. Ambiguities resulting from simultaneous weight loss due to water were minimized by initially calcining these samples in He to 970°C. This pre-treatment yields tungsten oxide on a transitional alumina (mostly θ) possessing a surface area of ~ 80 m²/gm. The retardation of WO_3 reduction depends on loading levels. At low loading levels (<8%), little or no reduction occurs. The 10% WO_3 on Al_2O_3 showed the first sign of reduction at 800°C. Although no weight loss was detected by TG, a slight greyish discoloration indicated some reduction had occurred. In contrast, bulk WO_3 is completely reduced after 2 hours at 600°C. Following 850 and 900°C reductions, 10% WO_3 on Al_2O_3 was extensively reduced and the presence of tungsten metal was confirmed by x-ray diffraction measurements.

ESCA. ESCA measurements also reveal the reduction resistance of the tungsten oxide surface phase on Al_2O_3 . An oxidized tungsten foil serves as a standard for the ESCA reduction experiments. The ESCA W 4f_{5/2,7/2} spectra for the oxidized, partially reduced and fully reduced tungsten foil are presented in Figure 1. The ESCA W 4f_{7/2} binding energy for the oxidized foil occurs at ~ 36 eV and corresponds to tungsten in the +6 oxidation state (17-19). The completely reduced foil exhibits an ESCA W 4f_{7/2} peak at ~ 32 eV corresponding to metallic tungsten (17-19). The partially reduced tungsten foil displays a very broad W 4f_{5/2,7/2} ESCA spectrum. Deconvolution of the ESCA W 4f signal from the partially reduced sample reveals the presence of five oxidation states of tungsten (W^{+6} , W^{+5} , W^{+4} , W^{+2} and W^0) (17,20). Thus, the reduction of bulk tungsten oxide to metallic tungsten proceeds through ESCA observable intermediate oxidation states of W^{+5} , W^{+4} , and W^{+2} .

The reduction behavior of a 60% WO_3 on Al_2O_3 sample as shown in Figure 2 was very similar to that observed for the oxidized tungsten foil. The ESCA W 4f_{7/2} binding energy for the oxidized sample occurs at ~ 36 eV and reveals that tungsten is present as W^{+6} . During partial reduction of the 60% WO_3 on Al_2O_3 sample the ESCA W 4f signal broadens indicating that in addition to W^{+6} and W^0 other oxidation states are present. However, the tungsten oxide in the 60% WO_3 on Al_2O_3 sample requires higher temperatures to completely reduce the tungsten oxide than tungsten oxide on the foil.

Figure 3 presents the ESCA W 4f spectra for the 10% WO_3 on Al_2O_3 sample. Note the higher temperatures required to initiate reduction for the supported tungsten oxide compared to the oxidized tungsten foil or the 60% WO_3 on Al_2O_3 sample. The W 4f_{7/2} binding energy for the oxidized sample occurs at ~ 36 eV and reveals that tungsten is present as W^{+6} . The tungsten oxide completely reduces to metallic tungsten at 900°C. Following this reduction the total intensity of the ESCA W 4f signal decreases by about 70%. X-ray diffraction shows the growth of large tungsten metal particles consistent with the decrease in the ESCA signal

Table I. Reduction Behavior of Tungsten Oxide on Alumina

After 900°C H ₂ Treatment (2 hr)					
% WO ₃	4	6	10	25	100
% Reduction (WO ₃ → W)	-0-	2.5%	49% ^a	85% ^b	Black
Color	White	Lt. Gray	Black	Black	Black
After 600°C H ₂ Treatment (2 hr)					
% WO ₃	4	6	10	25	100
% Reduction (WO ₃ → W)	-0-	-0-	-0-	~22% ^a	-100-
Color	White	White	White	Black	Black
10% WO ₃ /γ-Al ₂ O ₃ (2 hr at Reduction Temperature)					
Temperature °C	% Reduction WO ₃ → W		Color		
600	-0-		White		
700	-0-		White		
800	-0- ^c		Tint of Gray-Slight Discoloration		
850	17% ^a		Gray		
900	49% ^a		Black		

a. Reduction still continuing after 2 hr.

b. Some α-Al₂O₃ present.

c. Detection limit of 1 to 2%.

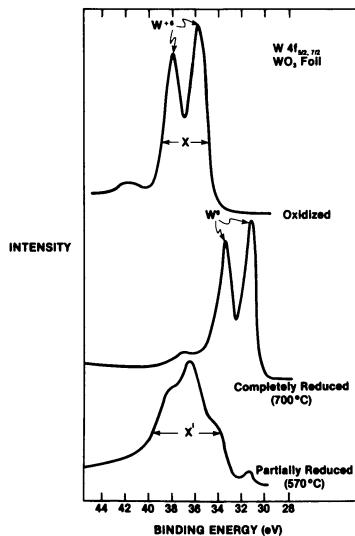


Figure 1. ESCA W 4f_{5/2, 7/2} spectra for a tungsten foil, oxidized and reduced. X indicates half width of oxidized sample; X' indicates half width of partially reduced sample.

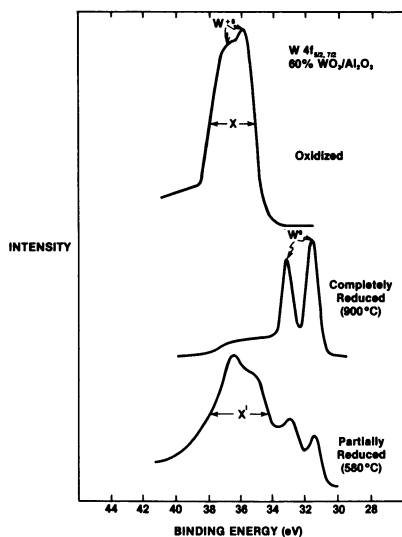


Figure 2. ESCA spectra for 60 Wt.% WO₃ on γ -Al₂O₃, oxidized and reduced. X indicates half width of oxidized sample; X' indicates half width of partially reduced sample.

intensity. For the partially reduced 10% WO_3 on Al_2O_3 sample the ESCA W 4f_{7/2} peak does not broaden suggesting the absence of W^{+5} , W^{+4} , and W^{+2} states. Deconvolution of the ESCA W 4f spectra for the partially reduced 10% WO_3 on Al_2O_3 sample only reveals the presence of W^{+6} and W^0 . Thus, the high temperature reduction of 10% WO_3 on Al_2O_3 does not proceed through ESCA observable intermediate tungsten oxidation state of W^{+5} , W^{+4} and W^{+2} .

RAMAN. The Raman spectra of WO_3 , $\text{Al}_2(\text{WO}_4)_3$, and 10% WO_3 on Al_2O_3 are presented in Figure 4. Crystalline WO_3 contains a distorted octahedral WO_6 network with the major vibrational modes at 808, 714 and 276 cm^{-1} . These modes have been assigned to W=O stretching, W=O bending and W-O-W deformation, respectively (21). Minor bands appear at 608, 327, 243, 218, 185 and 136 cm^{-1} . $\text{Al}_2(\text{WO}_4)_3$ (defect CaWO_4 structure) contains distorted, isolated tetrahedral tungsten groups. The major Raman peaks of $\text{Al}_2(\text{WO}_4)_3$ were assigned by comparison with tetrahedrally coordinated tungsten in a aqueous solution of WO_4^{2-} as well as with solid Na_2WO_4 (22). In Na_2WO_4 , the WO_4^{2-} groups are required to sit at crystallographically constrained tetrahedral sites (symmetry 42m). WO_4^{2-} (aq.) and Na_2WO_4 exhibit major vibrational modes at 938 and 928 cm^{-1} (symmetric W=O stretch), 830 and 813 cm^{-1} (antisymmetric W=O stretch), 324 and 312 cm^{-1} (W=O bending), respectively. Thus, the $\text{Al}_2(\text{WO}_4)_3$ peak at 1052 cm^{-1} is attributed to the W=O stretching mode and the doublet at 378-394 cm^{-1} is assigned to the W=O bending mode. Distortion in the tetrahedra dramatically affects the position of the bands.

The major Raman peak for 10% WO_3 on Al_2O_3 occurs around 970 cm^{-1} , and has been assigned to the W=O symmetrical stretch of the surface tungsten oxide species (19,23). The intensities of the major Raman band for WO_3 (808 cm^{-1}), $\text{Al}_2(\text{WO}_4)_3$ (1052 cm^{-1}), and 10% WO_3 on Al_2O_3 (970 cm^{-1}) were compared after normalization with respect to the laser power applied. The relative Raman intensity ratios for these peaks are 1600:40:1 for normalized laser power. These Raman intensity ratios were further scaled for the different tungsten oxide contents and yielded relative ratios of 160:5:1 (15).

The states of tungsten oxide on alumina depend on the tungsten oxide content and the temperature of calcination. The effect of tungsten oxide content is shown in Figures 5 and 6 for 15 and 25% WO_3 on Al_2O_3 , whereas the effect of changing temperatures with constant WO_3 content is shown in Figure 7. Figures 5a and b show Raman spectra of 15% and 25% WO_3 on Al_2O_3 calcined (with 8% steam present) at 760°C. Both materials exhibit surface areas of 120 m^2/gm . The 15% WO_3 on Al_2O_3 sample, Figure 5a, exhibits Raman bands of both a surface tungsten oxide species on the alumina support and a trace amount of crystalline WO_3 . The 25% WO_3 on Al_2O_3 sample, Figure 5b, however, shows very intense crystalline WO_3 Raman bands which dominate the spectrum due to the large Raman cross-section of this phase. The intensities of the Raman bands resulting from surface tungsten oxide species are similar for both of these samples as shown in Figure 6 after scaling for the different applied laser powers over the region 850-1150 cm^{-1} (15).

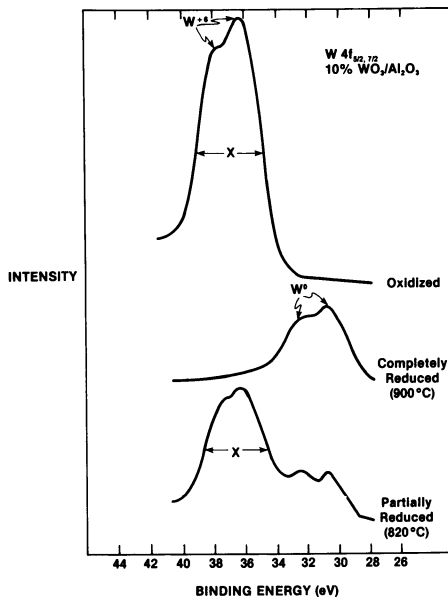


Figure 3. ESCA spectra for 10 Wt.% WO₃ on γ -Al₂O₃, oxidized and reduced. X indicates half width of oxidized sample; X' indicates half width of partially reduced sample.

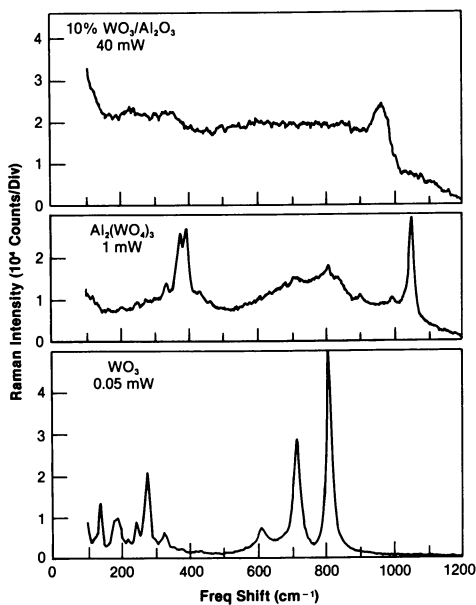


Figure 4. Laser Raman spectra of 10% WO₃ on Al₂O₃, aluminum tungstate and tungsten oxide.

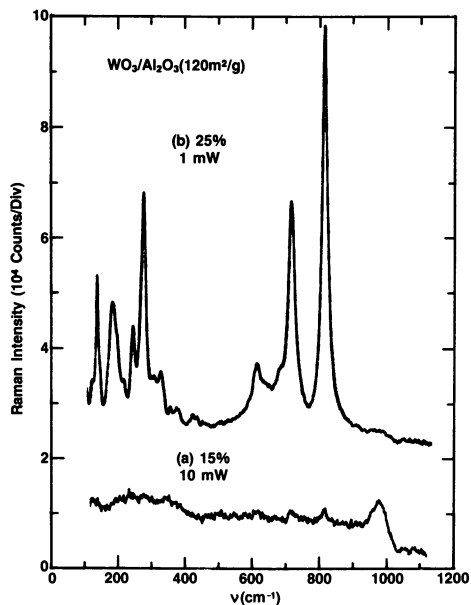


Figure 5. Laser Raman spectra of 25 Wt.% WO_3 on $\gamma\text{-Al}_2\text{O}_3$ and 15 Wt.% WO_3 on $\gamma\text{-Al}_2\text{O}_3$ de-surfaced to $120 \text{ m}^2/\text{g}$ surface area.

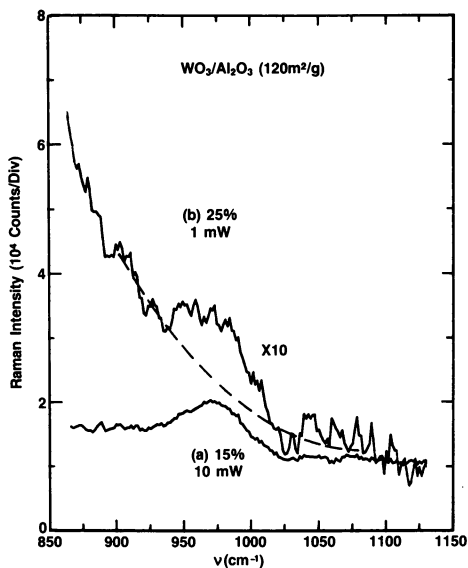


Figure 6. Laser Raman spectra from 850 to 1150 cm^{-1} of 25 Wt.% WO_3 on $\gamma\text{-Al}_2\text{O}_3$ and 15 Wt.% WO_3 on $\gamma\text{-Al}_2\text{O}_3$ de-surfaced to $120 \text{ m}^2/\text{g}$ surface area.

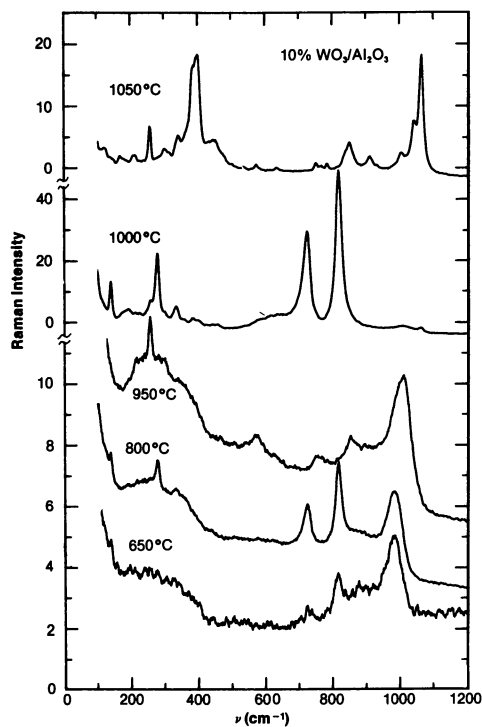


Figure 7. Laser Raman spectra of 10% WO_3 on $\gamma\text{-Al}_2\text{O}_3$ calcined at 450, 800, 950, 1000 and 1050°C.

The states of tungsten oxide on alumina were investigated over a wide temperature range (650-1050°C) for 10% WO₃ on Al₂O₃. The 10% WO₃ on Al₂O₃ sample calcined at 650°C exhibits Raman peaks at 972, 809 and 718 cm⁻¹. The peak near 970 cm⁻¹ is associated with a tungsten oxide surface complex (8,19,23). The position of this Raman peak shifts monotonically from 970 to about 1000 cm⁻¹ as the calcination temperature is increased to 950°C. Similar shifts are observed when tungsten oxide loading is increased for samples calcined at 500°C (7,19).

Samples calcined at 1000 and 1050°C display bulk tungsten oxide WO₃ and Al₂(WO₄)₃ phases. Raman peaks at 811, 717, 273 and 137 cm⁻¹ are characteristic of crystalline WO₃. These peaks decrease in intensity as the calcination temperature increases from 650-950°C, so that at 950°C the crystalline WO₃ Raman peaks at 811, 717 and 273 cm⁻¹ are absent. At 1000°C these peaks appear again, and then disappear following a calcination at 1050°C.

The major Raman peak of the Al₂(WO₄)₃ at 1055 cm⁻¹ is first observed following a calcination at 1000°C and dominates the Raman spectra after a 1050°C calcination. The θ-Al₂O₃ Raman peak at 253 cm⁻¹ is present in the spectra of samples calcined at 950-1050°C and agrees with X-ray diffraction. This series of Raman spectra reveals the dynamic nature of the WO₃ on Al₂O₃ system and its dependence upon calcination temperature.

Discussion

The strong interaction of WO₃ with a γ-Al₂O₃ surface modifies the behavior of both tungsten oxide and alumina. γ-Al₂O₃ will transform from a series of closely related transitional alumina phases possessing a defect spinel structure, containing both tetrahedral and octahedral aluminum ions, to α-Al₂O₃, a corundum structure containing only octahedral aluminum ions (24). The γ to α-Al₂O₃ transformation occurs by the condensation of surface hydroxyl groups and the elimination of H₂O. TG studies on powder samples, as well as, CAEM studies on model film systems indicate that WO₃ inhibits the γ to α-Al₂O₃ phase transformation. The presumed bonding of WO₃ with the hydroxyl surface of γ-Al₂O₃ blocks the transformation to α-Al₂O₃ (8). At sufficiently high temperatures (~1150°C) and high WO₃ concentrations, approximately 3X monolayer coverage (19), CAEM detects the reaction of tungsten oxide with alumina forming Al₂(WO₄)₃. Monolayer coverage is defined as 4.3x10¹⁸ W atoms/m² or 7 micromoles/m². A monolayer of WO₃ on γ-Al₂O₃ simply refers to the surface phase oxide structure at maximum packing of the alumina surface before crystallites of WO₃ are formed (15,19). The observation of the sequential formation of WO₃ followed by Al₃(WO₄)₃ is supported by the Raman studies (10,15,19).

Bulk WO₃ crystallizes in a distorted version of the ReO₃ structure with WO₆ octahedra linked via corner-sharing with neighboring WO₆ octahedra. Some thirty years ago, Magneli discovered that during reduction, WO₃ behaves in a nonclassical manner. As oxygens are removed, the WO₃ structure rearranges maintaining the metal coordination at six. During this process, the octahedra restructure along crystallographic shear planes to

share edges in place of corners. This tightened packing allows the structure to retain its metal coordination number at six even though the cation-to-anion ratio increases. In this way, partially-reduced WO_3 exists over a wide compositional range (25) with formal tungsten oxidation states of 5 and 6 and tungsten coordination of 6. Further reduction produces a discrete (WO_2) phase which displays a distorted rutile structure. WO_2 , which contains a distorted octahedral coordination about tungsten also reduces via a series of shear planes with tungsten assuming formal valence states of 3 and 4. Thus during the reduction of bulk WO_3 , intermediate oxidation states occur. Consistent with this mechanism (20), ESCA observes several intermediate oxidation states (+5, +4 and +2) during the reduction of bulk WO_3 , see Fig. 1.

The reduction behavior of tungsten oxide supported on $\gamma-Al_2O_3$ differs significantly from that of bulk WO_3 . TG studies of WO_3 on $\gamma-Al_2O_3$ show that below a coverage of 6% WO_3 , the surface tungsten oxide phase is essentially irreducible (10). At intermediate loadings (~10%), WO_3 partially reduces; while, at higher loadings (25%), the additional WO_3 behaves like bulk WO_3 , see Table I. We would suggest that the isolated surface tungstate groups (8,16,19,26) on the low loaded samples do not reduce through intermediate structures but, as our ESCA results indicate, the reduction proceeds directly to tungsten metal. Since reduction also occurs only at high temperature, the tungsten metal formed rapidly sinters into large particles.

Our high temperature reduction experiments using ESCA agree with both our TG studies and the recent low temperature reduction experiments reported by Salvati, et al. (19). Salvati and co-workers found a loading level dependence on reduction and the presence of bulk-like WO_3 species above a critical coverage. Our study (see Fig. 3) indicates that at the temperature necessary to reduce the surface phase of tungsten oxide on Al_2O_3 the reduced tungsten rapidly sinters to metallic particles (10). Apparently, the highly-dispersed state of the tungsten oxide complex on the alumina surface (8,19,26) precludes the formation of nonstoichiometric tungsten oxide phases which form during the reduction of unsupported WO_3 .

For WO_3 on Al_2O_3 samples containing more than a monolayer the additional tungsten oxide is present as WO_3 crystallites. These WO_3 crystallites are not in direct contact with the alumina support and are indistinguishable from bulk WO_3 in their reduction behavior (19,20). The WO_3 crystallites reduce at mild temperatures and exhibit ESCA observable intermediate tungsten oxidation states. Detailed analysis (20) of the 10% WO_3 on Al_2O_3 ESCA W 4f_{5/2,7/2} spectra in Figure 3 only reveals the presence of W^{+6} and $W^{0.5/2,7/2}$ on the alumina support after partial reduction. Within the experimental limits of ESCA, the high temperature reduction of the tungsten oxide surface complex on the alumina support does not proceed through observable intermediate tungsten oxidation states of W^{+5} , W^{+4} and W^{+2} , but rather directly from W^{+6} to W^0 . The different reduction behavior of the WO_3 crystallites and the tungsten oxide monolayer can be used to distinguish between these two forms of tungsten oxide on

alumina. Salvati et al. also used this approach to distinguish between the tungsten oxide surface complex and the WO_3 crystallites (19). Below monolayer coverage, tungsten oxide on alumina is not reduced after 12 hours at 550°C, but above monolayer coverage reduction of W^{+6} to W^0 at this temperature is observed with ESCA.

The TG and ESCA technique have shown evidence for a strong metal oxide-support interaction between WO_3 and $\gamma-Al_2O_3$ under high temperature reducing conditions. As we will now discuss CAEM and Raman spectroscopy suggest a strong interaction between WO_3 and $\gamma-Al_2O_3$ under high temperature oxidizing conditions, as well. Dynamic studies by CAEM of WO_3 on $\gamma-Al_2O_3$ at high temperature have been carried out for one-half and 3X monolayer loadings (19) of WO_3 on a model $\gamma-Al_2O_3$ film support. Following an *in situ* decomposition in oxygen of the ammonium meta-tungstate at 500°C on the 4 micromole/m² loaded film (about one-half monolayer) electron diffraction confirmed the presence of only transitional alumina phases (no α -phase was present). Heating this film to 1050°C shows no crystallization of the support; whereas with pure alumina films CAEM detects restructuring of the film to form $\alpha-Al_2O_3$ at this temperature. The particle size of the tungsten oxide phase for the one-half monolayer covered film at 500°C lies below the resolution limit (2.5 nm) of the microscope. Even upon continued heating to 1050°C WO_3 particles are still not visible, and the support does not transform to $\alpha-Al_2O_3$. This result suggests the presence of a highly-dispersed WO_3 phase stabilizes the alumina support from restructuring to $\alpha-Al_2O_3$.

When the more highly loaded WO_3 on alumina specimen, i.e. 3X monolayer coverage, was heated in oxygen, particles were detected by CAEM at 500°C. Because the size of these particles (3 nm) are near the resolution limit of the CAEM, we could not determine a detailed particle size analysis. As the temperature was raised to 700°C the WO_3 particles grow in diameter to between 5 and 10 nm. Detailed examination shows a nearly uniform distribution of the particles across the support. The particles have irregular angular shapes, but in many cases remained thin enough to avoid masking the structural features of the underlying support. This morphology is similar to that proposed for FeO "raft" structures on SiO_2 (27). The particles do not change size, shape or position upon further heating at 1050°C for 1 hr. Maintenance of particle identity indicates a strong interaction between particles and support (27,28).

As the temperature was raised from 1050°C to 1150°C the specimen with the higher WO_3 loading changes dramatically in appearance. Initially, the electron scattering density of the particles increases. While maintaining their 5 to 10 nm lateral dimensions, the particles apparently become thicker. As the change proceeds, the area of the alumina support surrounding the tungsten oxide particles becomes progressively more transparent to the electron beam, suggesting that Al_2O_3 preferentially leaves these areas and forms $Al_2(WO_4)_3$. Subsequent examination of specimens in the high resolution transmission electron microscope (where defocusing and tilting experiments were performed) confirm this phenomena and eliminate any question of over-focus or phase contrast artifacts (29,30).

In summary, at sufficiently high temperatures and high WO_3 concentrations, the CAEM follows the agglomeration of WO_3 into thin oxide cluster structures (26,27), which subsequently react with Al_2O_3 forming $Al_2(WO_4)_3$. Figure 8 outlines the proposed stepwise interaction of tungsten oxide with transitional $\gamma-Al_2O_3$ films.

Laser Raman spectroscopic studies of alumina-supported WO_3 catalysts have shown that three different tungsten oxide phases are present: WO_3 , $Al_2(WO_4)_3$, and a surface tungsten oxide species (8,19), Figure 4. The concentrations of these phases in WO_3 on Al_2O_3 catalysts depend on tungsten oxide loading and temperature of calcination (8). Previous studies have shown that Raman spectroscopy is more sensitive to WO_3 and $Al_2(WO_4)_3$ than to the surface tungsten oxide complex (8,19). No attempt, however, had been made to estimate the relative Raman cross sections of these tungsten oxide phases. This information would be useful to develop a model for the WO_3 on Al_2O_3 system (15).

The dynamic changes of tungsten oxide that occur on the surface of $\gamma-Al_2O_3$ as a function of calcination temperature and tungsten oxide content were followed by Raman spectroscopy for 10%, 15% and 25% WO_3 on $\gamma-Al_2O_3$ as described in the Results section. The Raman spectra of 15% WO_3 and 25% WO_3 on $\gamma-Al_2O_3$ calcined at 760°C, Figure 5 and 6 exhibits similar intensities for the bands of the surface tungsten oxide complex although the band intensities for crystalline WO_3 differ dramatically. Since the 15% WO_3 on $\gamma-Al_2O_3$ sample calcined at 760°C contains near monolayer coverage (19,26) the 25% WO_3 on $\gamma-Al_2O_3$ sample at this same temperature must contain crystallites of WO_3 . Raman spectroscopy confirms that the surface phase tungsten oxide complex will form WO_3 crystallites as the tungsten oxide content increases (at a constant surface area) beyond monolayer coverage (19,26).

The study of the 10% WO_3 on $\gamma-Al_2O_3$ as a function of temperature also reveals changing states of tungsten oxide, Figure 7. Initially this sample contains tungsten oxide below monolayer coverage, but as the temperature is raised and the surface area collapses, the tungsten oxide concentration exceeds monolayer coverage (19,26). The crossover point of approximate monolayer coverage occurs between 60 to 100 m^2/gm and is generated by calcination temperatures between 850 and 950°C.

Below monolayer coverage (less than ~25-30% WO_3 on Al_2O_3 of 200 m^2/g) tungsten oxide is primarily in a highly dispersed and amorphous state on the alumina surface and remains so at low calcination temperatures (500-800°C) (8,19,23,26). For 10% WO_3 on Al_2O_3 , Figure 7, the surface tungsten oxide complex is present up to 950°C. In addition, Raman peaks for crystalline WO_3 are also observed in this temperature range. The WO_3 crystallite concentration is low since they are not detected by X-ray diffraction. The amount of tungsten oxide present as crystalline WO_3 for 10% WO_3 on $\gamma-Al_2O_3$, Figure 7, is estimated to be less than 1% of the total tungsten oxide content present in the 10% sample calcined at 650 and 800°C (16). As the calcination temperature increases, the relative amount of crystalline WO_3 initially

decreases, as measured by the intensity ratio $I(811\text{ cm}^{-1})/I(965\text{--}1000\text{ cm}^{-1})$, (15). Thus, at the higher calcination temperatures a substantial decrease in the surface area of the alumina support occurs and simultaneously the WO_3 particles disperse to form the tungsten oxide surface complex. As the surface area decreases the distance between the tungsten oxide surface species decreases and the tungsten oxide surface density on the alumina support increases (19,26). The increase in the intensity of the ESCA $W\ 4f_{5/2,7/2}$ signal (19,26) and the shift from ~ 965 to $\sim 1000\text{ cm}^{-1}$ in the Raman band associated with the tungsten oxide surface complex (16) reflect this change. These structural changes in the WO_3 on Al_2O_3 system are depicted in Figures 9a and 9b. Thus, Raman spectroscopy confirms that the surface phase tungsten oxide complex will form WO_3 crystallites as the alumina desurfaces (at a constant tungsten oxide content), and monolayer coverage is exceeded.

A close-packed monolayer of tungsten oxide on alumina apparently forms when the minimum distance between non-polymeric tungsten oxide centers is achieved (8,19,26). The formation of the close-packed tungsten oxide monolayer, however, does not preclude the alumina from additional loss in surface area at still higher temperatures. The close-packed tungsten oxide monolayer accommodates further de-surfacing by forming bulk tungsten oxide phases WO_3 and $\text{Al}_2(\text{WO}_4)_3$ (see Figures 9c and 9d). The formation of WO_3 and $\text{Al}_2(\text{WO}_4)_3$ crystallites at higher temperatures is detected by laser Raman spectroscopy, Figure 7.

The CAEM studies indicate that at high temperatures the surface tungsten oxide phase transforms to thin WO_3 particles. These in turn react at high temperatures with the underlying alumina support to form $\text{Al}_2(\text{WO}_4)_3$. Thus both CAEM and Raman spectroscopy point to the same model for the transformation of the tungsten oxide surface phase; first to form tungsten oxide particles and then to form subsequently $\text{Al}_2(\text{WO}_4)_3$ at high temperature calcination conditions.

Conclusions

The strong interaction between WO_3 and $\gamma\text{-Al}_2\text{O}_3$ manifests itself under both high temperature reducing and oxidizing conditions. Under reducing conditions, TG and ESCA demonstrate that the critical coverage for virtual non-reducibility of WO_3 on an alumina surface (which has been exposed to high temperature and de-surfaced to $\sim 80\text{ m}^2/\text{gm}$) is 6-8 wt.%. Above this monolayer coverage more easily reduced bulk-like WO_3 species are present. For loadings of 10 wt.%, where partial reduction occurs at high temperature, the tungsten oxide appears to reduce directly from W^{+6} to W^0 without accessing the intermediate oxidation states that bulk WO_3 passes through.

Under high temperature oxidizing conditions, laser Raman spectroscopy and CAEM demonstrate the dynamic behavior of the amorphous and crystalline structural transformations occurring in the WO_3 on Al_2O_3 system. Below monolayer coverage of tungsten oxide on alumina, the tungsten oxide phase is present as a highly dispersed and amorphous surface complex on the support. Above

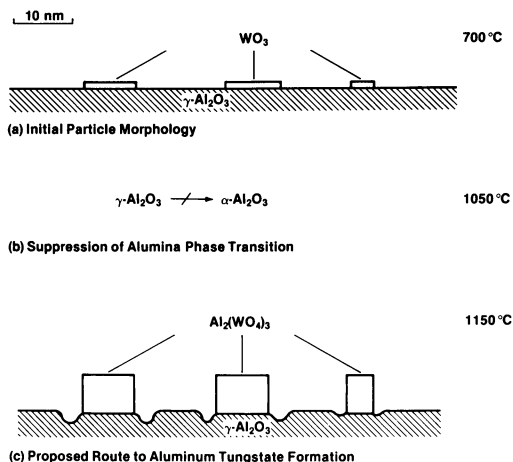


Figure 8. Model of the transformations observed for tungsten oxide on an alumina film by controlled atmosphere electron microscopy.

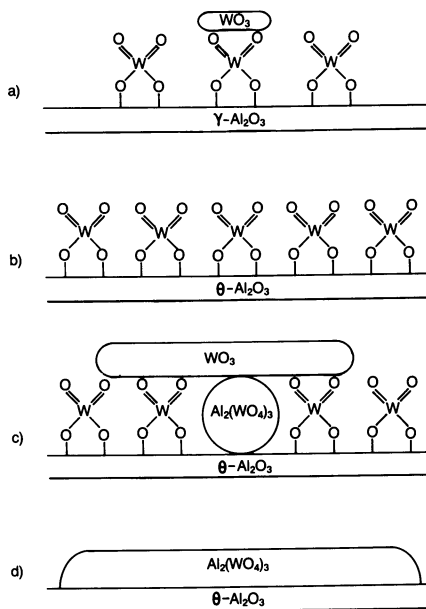


Figure 9. Model of the structure/transformations of tungsten oxide on high surface area $\gamma\text{-Al}_2\text{O}_3$ as a function of calcination temperature.

monolayer coverage, both a surface complex and discrete WO_3 crystallites are present. During high temperature de-surfacing a portion of the surface complex converts first to WO_3 and then reacts with the alumina to form $Al_2(WO_4)_3$.

Literature Cited

1. Tauster, S. J.; Fung, S. C.; Baker, R. T. K.; Horsley, J. A. Science 1981, 211, 1121.
2. Chen, B. H.; White, J. M.; Brostrom, L. R.; Deviney, M. L. J. Phys. Chem. 1983, 87, 2423.
3. Reymond, J. P.; Meriaudeau, P.; Teichner, S. J. J. Catal. 1982, 75, 39.
4. Topsoe, H.; Dumesic, J. A.; Morup, S. In "Applications of Mossbauer Spectroscopy"; Cohen, R. L., Ed.; Academic Press: New York, 1980; Vol. II.
5. Murrell, L. L.; Garten, R. L. (in press).
6. Hogan, J. P. J. Poly. Sci. 8(A-1) 1970, 2637.
7. Thomas, R.; Kerkhof, F. P. J. M.; Moulijn, A. J.; Medema, J.; deBeer, V. H. J. J. Catal. 1980, 61, 559.
8. Tittarelli, P.; Iannibello, A.; Villa, P. L. J. Sol. St. Chem. 1981, 37, 95.
9. Thomas, R.; deBeer, V. H. J.; Moulijn, J. A. Bull. Soc. Chim. Belg. 1981, 90(12), 1349.
10. Soled, S.; Murrell, L.; Wachs, I.; McVicker, G. Am. Chem. Soc. Div. Pet. Chem. Prepr. 1983, 28, 1310.
11. Baker, R. T. K.; Harris, P. S. J. Sci. Instrum. 1972, 5, 793.
12. Wagner, C. D.; Riggs, W. M.; Davis, L. E.; Moulder, J. F.; Muilenberg, G. E. "Handbook of X-Ray and Photoelectron Spectroscopy"; Physical Electronics Industries 1979.
13. Mettler Technical Bulletin, TA-2000C, Hightstown, N.J., 1980.
14. Soled, S.; McVicker, G. B.; DeRites, B. Proceedings 11th NATAS Conf., 1981, 417.
15. Chan, S. S.; Wachs, I. E.; Murrell, L. L. (in press).
16. McVicker, G. B.; Garten, R. L.; Baker, R. T. K. J. Catal. 1978, 54, 129.
17. Haber, J.; Stock, J.; Ungier, L. J. Sol. St. Chem. 1976, 19, 113.
18. Salje, E.; Carley, A. F.; Roberts, M. W. J. Sol. St. Chem. 1979, 29, 237.
19. Salvati, L.; Makovsky, J. M.; Stencel, J. M.; Brown, F. R.; Hercules, D. M. J. Phys. Chem. 1981, 85, 3700.
20. Wachs, I. E.; Chersich, C. C.; Hardenbergh, J. H. (in press).
21. Anderson, A. Spectr. Lett. 1976, 9, 809.
22. Busey, R. H.; Keller Jr., D. L. J. Chem. Phys. 1964, 41, 215.
23. Thomas, R.; Moulijn, J. A.; Kerkhof, F. P. J. M. Recl. Trav. Chim. Pays-Bas 1977, 96, M134.
24. Knozinger, H.; Ratnasamu, P. Catal. Rev-Sci. Engr. 1978, 17(1), 31.
25. Wells, A. F. Structural Inorganic Chemistry, Oxford Press, London 1962.
26. Murrell, L. L.; Grenoble, D. C.; Baker, R. T. K.; Prestridge, E. B.; Fung, S. C.; Chianelli, R. R.; Cramer, S. P. J. Catal. 1983, 79, 203.

27. Yuen, S.; Chen, Y.; Kubsh, J. E.; Dumesic, J. A.; Topsoe, N.; Topsoe, H. J. Phys. Chem. 1982, 86, 3022.
28. Baker, R. T. K.; Prestridge, E. G.; Garten, R. L. J. Catal. 1979, 56, 390.
29. Flynn, P. C.; Wanke, S. E.; Turner, P. S. J. Catal. 1974, 33, 233.
30. Treacy, M. M. J.; Howie, A. J. J. Catal. 1980, 63, 265.

RECEIVED October 4, 1984